Nano Energy 54 (2018) 17–25

Contents lists available at ScienceDirect

Nano Energy

journal homepage: www.elsevier.com/locate/nanoen

Communication

Ionic liquid-immobilized polymer gel electrolyte with self-healing capability, high ionic conductivity and heat resistance for dendrite-free lithium metal batteries

Tao Chen[a], Weihua Kong[a], Zewen Zhang[a], Lei Wang[a], Yi Hu[a], Guoyin Zhu[a], Renpeng Chen[a], Lianbo Ma[a], Wen Yan[a], Yanrong Wang[a], Jie Liu[a,b], Zhong Jin[a,*]

[a] Key Laboratory of Mesoscopic Chemistry of MOE, School of Chemistry and Chemical Engineering, Nanjing University, Nanjing, Jiangsu 210023, China
[b] Department of Chemistry, Duke University, Durham, NC 27708, United States

ARTICLE INFO

Keywords:
Lithium metal batteries
Self-healing capability
Polymer gel electrolyte
Self-discharge

ABSTRACT

High-energy rechargeable lithium metal batteries have attracted soaring attention because of high specific capacity and low electrochemical potential of lithium metal. Unfortunately, the lithium dendrite growth upon Li plating severely hinders its practical application. Herein, we report the preparation of ionic liquid (IL) immobilized polymer gel electrolytes with strong ion-dipole interactions between imidazolium-based IL and fluorinated copolymer gel for stable and dendrite-free Li^+ plating/stripping. The adoption of IL leads to the formation of a tightly cross-linked gel framework with tethered anions, providing greatly-improved mechanical strength, good heat resistance, favorable self-healing capability, high ionic conductivity, and a stable electrochemical window up to 4.5 V vs. Li^+/Li that can satisfy the demand of high-voltage cathodes. The membrane of IL-immobilized polymer gel electrolyte enabled dendrite-free Li deposition, showing stable cycling durability for 1000 h at 0.5 mA cm^{-2}, and the functional mechanism was carefully investigated. By coupling with this gel electrolyte membrane, the $LiFePO_4$/Li cell exhibit much superior cycling stability and rate performance. Moreover, the lithium-sulfur batteries assembled with the IL-immobilized polymer gel electrolyte also show efficient suppression of polysulfide shuttling and self-discharge, bringing high specific capacity and long cycling life.

1. Introduction

In the past few decades, the ever-growing demands for high-energy-density batteries have impelled the flourish of new battery technologies [1]. Lithium metal has been regarded as an ideal anode material for developing next-generation lithium batteries (such as lithium-sulfur and lithium-air batteries), because of its ultrahigh specific capacity (3860 mAh g^{-1}) and low reduction potential (−3.040 V vs. standard hydrogen electrode, SHE) [2–4]. However, the safety problem caused by uneven and unmanageable growth of Li dendrites during Li plating processes hinders the development of lithium metal-based rechargeable batteries [5]. Another issue is the formation of unstable solid-electrolyte interphase (SEI) resulted from the consumption of electrolyte and lithium metal anode, leading to the increase of interfacial resistance and safety risks (i.e., internal short-circuits and explosion) [6–8].

To suppress the growth of Li dendrites and stabilize the SEI film, various strategies, such as the introduction of electrolyte additives [9,10], solid or quasi-solid electrolytes [11–17], separator modifications [18,19] and lithium metal hosts [20–22], have been proposed. Among these attempts, solid or gel electrolytes have drawn ever-increasing attention because they can make good interfacial contact with Li electrode and effectively block the growth and penetration of Li dendrites [23,24]. In comparison with solid-state inorganic electrolytes, polymer gel electrolytes exhibit superior flexibility and film-forming processability [25]. Furthermore, an ideal polymer gel electrolyte for lithium metal batteries should possess the following properties: (1) high ionic conductivity at room temperature, (2) good mechanical strength to prevent Li dendrite growth, (3) wide operation voltage window for stable discharge-charge cycling [25–30]. To improve the mechanical strength, a common strategy is introducing inorganic nanofillers (e.g. SiO_2 [31–33], Al_2O_3 [34], and TiO_2 [35]) into the matrix of polymer gel electrolyte. However, the agglomeration of these non-Li^+-conductive nanoparticles may block ion transport pathways, thus resulting in unsatisfactory ionic conductivity. Therefore, it is highly desirable to find

* Corresponding author.
E-mail address: zhongjin@nju.edu.cn (Z. Jin).

https://doi.org/10.1016/j.nanoen.2018.09.059
Received 9 July 2018; Received in revised form 1 September 2018; Accepted 25 September 2018
Available online 25 September 2018

an effective strategy for fabricating polymer gel electrolytes with improved Li-ion conducting properties and strong dendrite-suppressing ability. Recently, Archer and coworkers demonstrated that the addition of ionic liquid (IL) into conventional organic solution (liquid) electrolyte can stabilize lithium anode against Li dendrite growth [36,37]. Theoretical studies also confirmed that tethered anions in ILs can improve the plating stability of lithium metal anode [38,39]. Moreover, the anion-tethered ILs can offer a localized reservoir of anions to mitigate the unstable electric field in the space-charge region near Li anode [38,39]. However, so far the present approaches are still limited by the high reactivity of Li metal and the formation of unstable SEI film in liquid electrolytes [40].

Here we propose that a viable strategy to replace organic solution electrolyte is to design IL-immobilized polymer gel electrolytes, which can provide high ionic conductivity, wide operation voltage window, good thermal stability, strong mechanical strength and helpful self-healing properties. To the best of our knowledge, there has been no report on the immobilization of ILs in polymer gel electrolytes via ion-dipole interactions for the homogeneous Li deposition and effective suppression of Li dendrite growth. To prepare IL-immobilized polymer gel electrolytes, we found that imidazolium salts (i.e., 1-ethyl-3-methylimidazolium bis(trifluoromethylsulfonyl)-imide, abbr. EMI-TFSI) can serve as a good choice of ILs because of their high ionic strength, high electrochemical stability and nonflammability [41]. On the other hand, fluorinated copolymers, such as poly(vinylidene fluoride-*co*-hexafluoropropylene) (P(VDF-HFP)) exhibit high dielectric constant, remarkable stability, high thermal endurance and strong mechanical strength, therefore can serve as flexible polymer gel matrix for constructing reliable quasi-solid electrolytes [42,43]. Moreover, the absorbed imidazolium ILs in P(VDF-HFP) copolymer gel lead to strong ion-dipole interactions between positively-charged imidazolium cations and partially negatively-charged fluorine atoms, thus can form a three-dimensional cross-linked network with tethered TFSI anions and favorable self-healing capability for enhancing the ionization of lithium salts, facilitating the transport of Li^+ ions and suppressing the growth of lithium dendrites.

2. Results and discussion

The fabrication process of IL-immobilized polymer gel electrolyte is illustrated in Scheme S1. Firstly, EMI-TFSI IL was immobilized into P(VDF-HFP) copolymer gel framework by the drop-casting of the mixed acetone solution of EMI-TFSI and P(VDF-HFP) to form a thin and uniform membrane, termed as IL-P(VDF-HFP). After vacuum-drying and putting into an Ar-filled glovebox, the membrane was further soaked into 1.0 M lithium bis(trifluoromethanesulphonyl)imide (LiTFSI) solution in a mixed solvent of dimethoxyethane/dioxolane (DME/DOL, 1:1 in volume) to obtain the gel electrolyte LiTFSI-IL-P(VDF-HFP). In this way, the main chains of P(VDF-HFP) were cross-linked by the ion-dipole interactions between the imidazolium cations and the polar $–CF_x$ groups of P(VDF-HFP). Compared to conventional organic solution electrolytes, the LiTFSI-IL-P(VDF-HFP) gel electrolyte with tethered TFSI anions can regulate the Li^+ flux near lithium anode to restrain Li dendrite growth during Li plating (Fig. 1). Moreover, the strong ion-dipole interactions in cross-linked IL-P(VDF-HFP) matrix result in enlarged amorphous regions and immobilized TFSI anions, thereby improving the ionic conductivity and widening the electrochemical voltage window. As detailed below, the LiTFSI-IL-P(VDF-HFP) gel electrolyte with remarkable flexibility also exhibits tight interfacial contact with electrode, and possesses intriguing self-healing properties than can thoroughly recover from severe mechanical damage/breakage.

As shown in Fig. 2**a**, the IL-P(VDF-HFP) membrane is transparent and mechanically flexible. The scanning electron microscopy (SEM) images of IL-P(VDF-HFP) shows a thickness of about 32 μm (Fig. 2**b**), and also exhibits a smooth surface and compact structure without any pinhole (Fig. 2**c**). The corresponding energy-dispersive X-ray spectroscopic (EDX) mappings of F, N, and S elements confirm the uniform distribution of EMI-TFSI (Fig. 2**d**). Benefited from the cross-linked P(VDF-HFP) matrix, the membrane exhibits prominent flexibility, which can provide tight interfacial contact with electrode. As a control sample, pristine P(VDF-HFP) membrane without adding EMI-TFSI IL was also fabricated. The X-ray diffraction (XRD) patterns of pristine P(VDF-HFP) and IL-P(VDF-HFP) were presented in Fig. 2**e**. The characteristic peaks of P(VDF-HFP) at 17.9°, 20.2°, 26.4°, and 38.7° confirm the presence of *α*-phase PVDF. After cross-linked with EMI-TFSI, the peak intensities of IL-P(VDF-HFP) are obviously reduced, indicating a decreased crystallinity and a higher degree of amorphous phase. The increased amorphous regions in IL-P(VDF-HFP) membrane are conducive to improve the Li^+ mobility and enhance the ionic conductivity. The chemical bonding states of P(VDF-HFP) and IL-P(VDF-HFP) were further elucidated by Fourier transform infrared spectroscopy (FTIR), as shown in Fig. 2**f**. The peaks at around 1398, 1180, and 884 cm^{-1} are attributed to CH_2 wagging, CF_2 antisymmetric stretching, and amorphous phase P(VDF-HFP), respectively [44]. After the introduction of EMI-TFSI, both the CH_2 wagging and CF_2 antisymmetric stretching peaks show obvious blue shift.

The formation of the cross-linked network can significantly enhance the maximum strain and Young's modulus of IL-P(VDF-HFP) membrane. The mechanical performance of the IL-P(VDF-HFP) membrane was measured using a strain-stress mechanical tester (Fig. S1). Along with the increase of IL to 40 wt%, the strain of gel electrolyte is significantly improved, whereas the maximum tensile stress decreases. This indicates that the ion-dipole interactions can reinforce the cross-linked network of the gel electrolyte. However, when the amount of IL further increases to 50 wt%, the maximum strain is slightly decreased, because the excess IL cannot further reinforce the cross-linked network of polymer matrix. The IL-P(VDF-HFP) membrane with 40 wt% EMI-TFSI shows the optimized maximum strain ratio. The surface morphology and Young's modulus of IL-P(VDF-HFP) membrane were further characterized by atomic force microscopy (AFM) with peak force tapping mode. The surface roughness of IL-P(VDF-HFP) membrane is only ca. 45 nm (Fig. S2), capable of strengthening the interfacial contact with electrode. Moreover, the IL-P(VDF-HFP) membrane presents a high Young's modulus of 6.8 GPa, which is 4 times higher than that of pristine P(VDF-HFP) (Fig. S2). This result confirms that the incorporation of IL into P(VDF-HFP) matrix can significantly improve mechanical strength due to the strong ion-polar crosslinking between IL cations and P(VDF-HFP). It has been predicted that solid electrolytes with Young's modulus higher than 6 GPa can sufficiently block Li dendrite formation and penetration [45]. Therefore, the IL-P(VDF-HFP) membrane is expected to be effective for the suppression of Li dendrite growth.

Thermal stability is very crucial to the electrolytes for use in lithium metal batteries. It is known than conventional ether-based solution electrolytes have poor heat resistance and are prone to fire and explosion upon short-circuits, high temperature and breakage. The flammability tests of conventional DME/DOL-based liquid electrolyte-soaked Celgard separator, LiTFSI-P(VDF-HFP) membrane and LiTFSI-IL-P(VDF-HFP) membrane are shown in Fig. S3. When the liquid electrolyte-soaked Celgard separator was placed close to fire, it immediately caught on fire and burned to ashes. Similarly, the LiTFSI-P(VDF-HFP) membrane also exhibited high flammability. On the contrary, LiTFSI-IL-P(VDF-HFP) membrane was difficult to catch fire and still well retained its original morphology. The low flammability of LiTFSI-IL-P(VDF-HFP) is mainly attributed to the nonflammability of EMI-TFSI IL and the stable cross-linked structure formed by strong ion-dipole interactions, which can greatly enhance the safety performance of rechargeable lithium metal batteries. Thermogravimetric analysis (TGA) results of Celgard separator, P(VDF-HFP) membrane and IL-P(VDF-HFP) membrane under air atmosphere are compared in Fig. S4. The Celgard separator suffered mass loss from 250 to 360 °C, owing to the rapid decomposition of the polypropylene. The corresponding weight loss

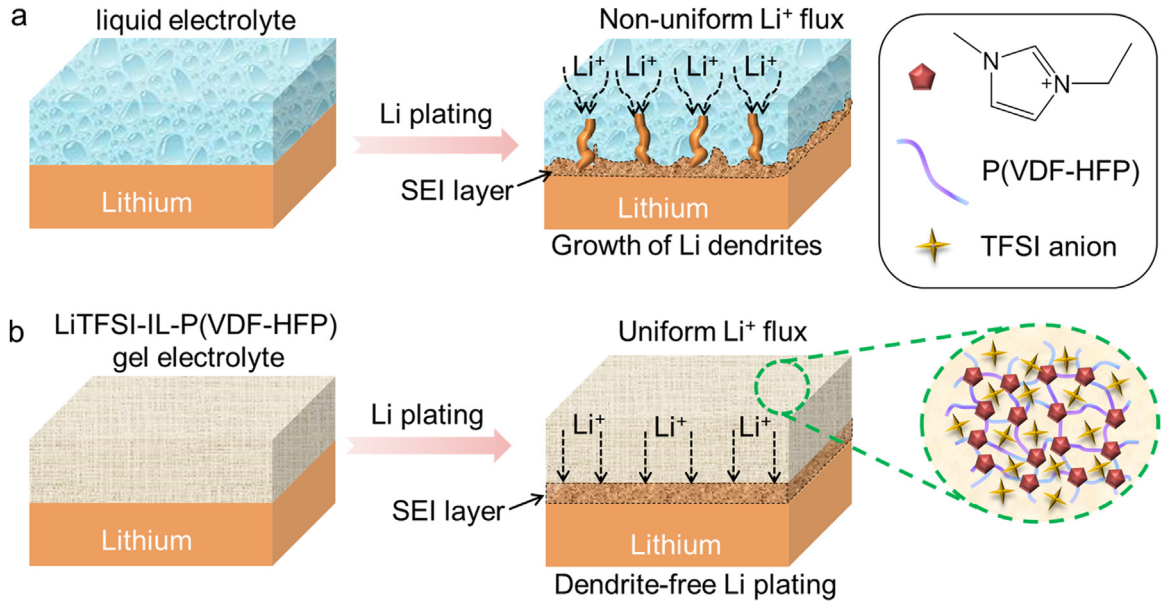

Fig. 1. (a) Schematic illustration of the electrochemical deposition behavior of lithium metal anodes with (a) liquid organic solution electrolyte and (b) LiTFSI-IL-P(VDF-HFP) gel electrolyte.

temperature range of P(VDF-HFP) membrane was 300–500 °C. For IL-P(VDF-HFP) membrane, the weight loss appeared between 450 and 550 °C, further confirming its high pyrolysis temperature.

To identify the self-healing capability, the pristine P(VDF-HFP) and IL-P(VDF-HFP) membranes were scratched with a razor blade and incubated in a mixed DME/DOL solution of 1.0 M LiTFSI. After being soaked for 12 h, the scratch on pristine P(VDF-HFP) membrane was just slightly healed (Fig. 2**g**). In contrast, the scratch on IL-P(VDF-HFP) was almost completely vanished after 12 h (Fig. 2**h**). In order to understand the self-healing mechanism and ion-dipole interactions, we also compared the FTIR spectra of pristine P(VDF-HFP) and IL-P(VDF-HFP) membranes with different contents of EMI-TFSI IL (Fig. S5). Upon the addition of EMI-TFSI, the peaks at 1398 cm^{-1} ($–CH_2$ wagging) and 1180 cm^{-1} ($–CF_2$ antisymmetric stretching) are gradually shifted to higher wavenumbers. This result suggests the strong interaction between the imidazolium cations and the C–F dipoles on the polymer chains.

The electrochemical stability of LiTFSI-IL-P(VDF-HFP) gel electrolyte was estimated by linear sweep voltammetry using a Li/LiTFSI-IL-P(VDF-HFP)/stainless-steel cell, shows a voltage window up to 4.5 V vs. Li^+/Li, which is wider than those of LiTFSI-P(VDF-HFP) gel and DME/DOL-based liquid electrolytes (Fig. S6). Electrochemical impedance spectroscopy (EIS) analysis was conducted to evaluate the Li-ion conductivity of LiTFSI-IL-P(VDF-HFP). Fig. S7a displays typical Nyquist plots of LiTFSI-IL-P(VDF-HFP) gel electrolytes with different EMI-TFSI contents (from 0 to 50 wt%). The ionic conductivity was calculated on the basis of the thickness and area of LiTFSI-IL-P(VDF-HFP). As the weight content of EMI-TFSI increases, the room-temperature ionic conductivity reaches the maximum value at 40 wt% (Fig. S8), mainly attributed to the formation of cross-linked network that reduces the crystallinity of P(VDF-HFP) matrix and increases the electrolyte uptake ratio. The LiTFSI-IL-P(VDF-HFP) with 50 wt% EMI-TFSI shows reduced ionic conductivity, probably because the excess IL decrease the effective Li^+ uptake. Fig. S7b shows the Arrhenius plots of LiTFSI-IL-P(VDF-HFP) gel electrolyte at different temperatures ranging from 25 to 75 °C, showing increased ion conductivity at elevated temperatures. The LiTFSI-IL-P(VDF-HFP) gel electrolyte with 40 wt% of EMI-TFSI exhibit high ionic conductivity of 8.8×10^{-4} S cm^{-1} at room temperature, comparable to that of liquid electrolyte-soaked Celgard separator ($\sim 4 \times 10^{-4}$ S cm^{-1}) [26]. The ionic conductivity of LiTFSI-IL-P(VDF-HFP) at 35, 45, 55, 65 and 75 °C are 1.5×10^{-3}, 2.6×10^{-3}, 3.6×10^{-3}, 4.6×10^{-3} and 5.5×10^{-3} S cm^{-1}, respectively, which are higher than those of LiTFSI-P(VDF-HFP) without immobilized EMI-TFSI. The activation energy E_a of LiTFSI-IL-P(VDF-HFP) was calculated according to the Arrhenius equation $\sigma(T) = A \exp(-E_a/RT)$. The low value of E_a reflects the faster transport of Li^+ ions in the electrolyte. With the increase of EMI-TFSI content, the E_a of LiTFSI-IL-P(VDF-HFP) gel electrolyte can reach the minimum value of 0.31 at 40 wt% of EMI-TFSI, indicating that the amorphous phase P(VDF-HFP) and suitably-immobilized TFSI anions may contribute to the fast Li^+ conduction.

To evaluate the compatibility of electrolytes with Li metal electrodes, galvanostatic Li plating/stripping cycling tests were performed with Li/Li symmetric cells. Fig. 3**a** displays the time-dependent voltage curves of the Li/Li symmetric cells with LiTFSI-IL-P(VDF-HFP) gel, LiTFSI-P(VDF-HFP) gel, and DME/DOL-based liquid electrolytes at a constant current density of 0.5 mA cm^{-2} for 2 h per each cycle. The Li/LiTFSI-IL-P(VDF-HFP)/Li cell exhibited a consistent low voltage polarization and a flat voltage plateau for 1000 h without short-circuiting, indicating that the LiTFSI-IL-P(VDF-HFP) gel electrolyte can effectively stabilize Li stripping/plating processes and suppress Li dendrite growth. In contrast, the voltage polarization in the Li/Li cell with DME/DOL-based liquid electrolyte was ~ 42 mV in the initial cycle and gradually increased to 190 mV after cycling for 268 h. The sudden voltage drop at 268 h indicates an internal short-circuit triggered by the penetration of dendritic Li growth. The Li/LiTFSI-P(VDF-HFP)/Li cell showed a longer cycling time (~ 400 h) than the Li/Li cell with liquid electrolyte. The Li plating/stripping stability of the symmetric cells with LiTFSI-IL-P(VDF-HFP) gel or DME/DOL-based liquid electrolytes at a higher current density of 2.0 mA cm^{-2} was also examined. The Li/LiTFSI-IL-P(VDF-HFP)/Li cell still exhibited low overpotential of 50 mV and good cycling stability up to 230 h (Fig. 3**b**), indicating the efficient suppression of electrode polarization and improved reaction kinetics. On the contrary, the Li/Li cell with liquid electrolyte showed a larger voltage hysteresis and a short-circuit after cycling for 125 h induced by the Li dendrite growth and penetration, owing to the nonuniform Li deposition and severe electrolyte decomposition. As shown in Fig. S9, the Li/Li symmetric cell with LiTFSI-IL-P(VDF-HFP) gel electrolyte shows the lowest impedance, indicating the stable interface resulted from LiTFSI-IL-P(VDF-HFP). The FTIR spectra of IL-P(VDF-HFP) membrane before and after Li plating/stripping tests show almost the same characteristic

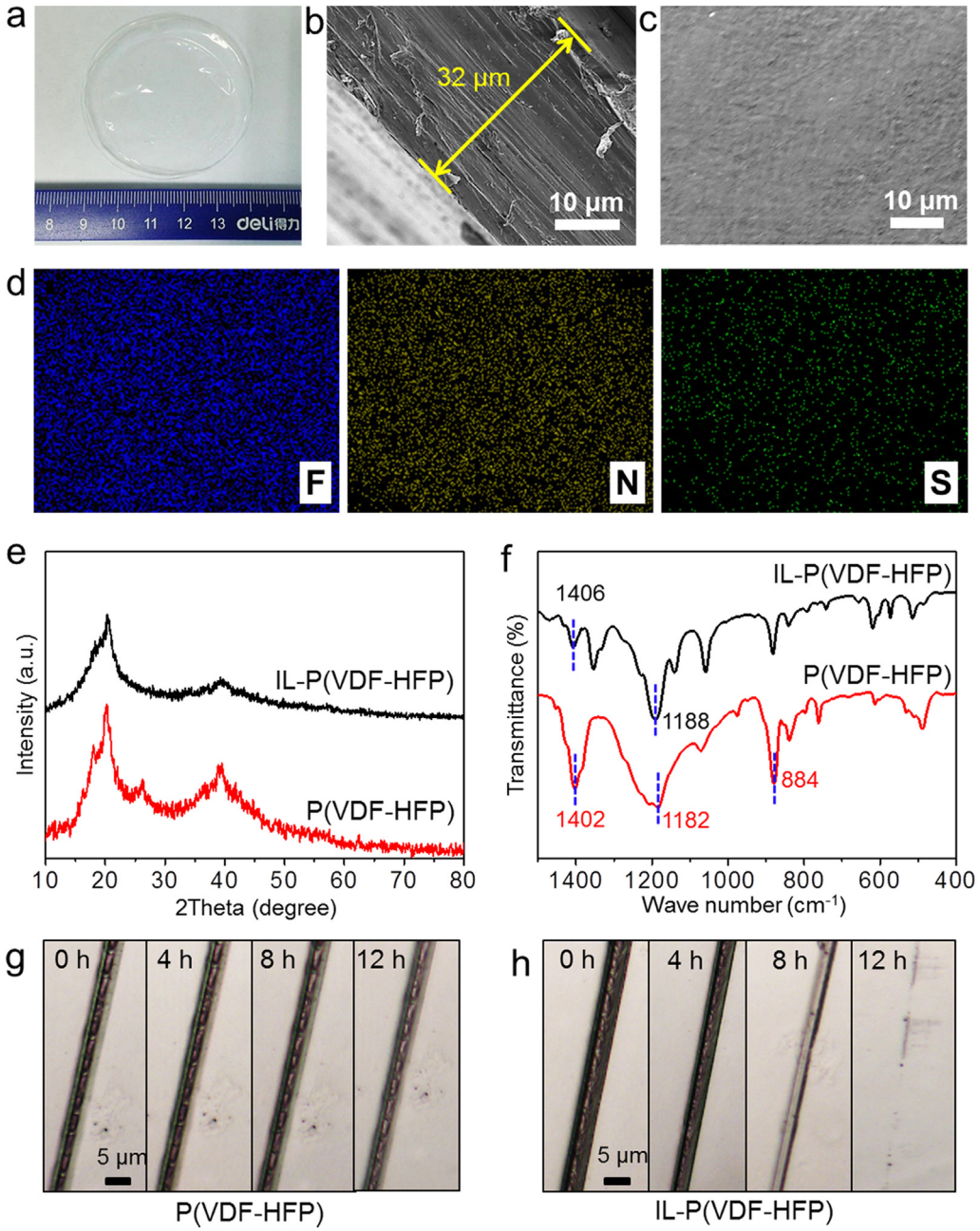

Fig. 2. (a) Optical photograph, (b) Cross-sectional SEM images and (c) surface SEM images of IL-P(VDF-HFP) membrane. (d) EDX mappings of F, N and S elements corresponding to (c). (e) XRD patterns and (f) FTIR spectra of pristine P(VDF-HFP) and IL-P(VDF-HFP) membranes. Optical microscopic observations of the self-healing capability of scratched (g) pristine P(VDF-HFP) and (h) IL-P(VDF-HFP) membranes after immersing in a mixed DME/DOL (1:1 in volume) solution of 1.0 M LiTFSI at room temperature for 0, 4, 8, and 12 h, respectively.

peaks, indicating that the IL-P(VDF-HFP) membrane is electrochemically stable during the cycling processes (Fig. S10). The Li/LiTFSI-IL-P(VDF-HFP)/Li cell also exhibited superior rate performance at various current densities of 0.5, 1.0, 2.0, and 4.0 mA cm^{-2} with a plating/stripping time of 1.0 h per cycle (Fig. S11). As the current density increased from 0.5 to 4.0 mA cm^{-2}, stable Li deposition can still be achieved for the symmetric cell with LiTFSI-IL-P(VDF-HFP) gel electrolyte, though with a little increase in voltage hysteresis. Long-term cycling stability was also examined at 1.0 mA cm^{-2} for a high areal capacity of 5 mAh cm^{-2} (Fig. 3**c**), and the cell exhibited stable voltage polarization without internal short-circuit after cycling for 1000 h. The voltage profiles between the time ranges of 160–170, 420–430, and 900–910 h present steady voltage hysteresis during Li plating/stripping cycles without obvious change in overpotential. These results indicate that LiTFSI-IL-P(VDF-HFP) gel electrolyte has remarkable dendrite-suppressing ability for high-performance lithium metal batteries. Notably, the optimized IL-PVH electrolyte in this work exhibit good cycling stability and dendrite-suppressing ability comparable with other recently reported polymer electrolytes (Table S1).

The morphology and compositions of SEI layers were characterized after complete Li stripping. The SEI layer formed by DME/DOL-based liquid electrolyte shows a rough and loose structure (Fig. 3**d** and S12a), which cannot well accommodate the volume change and dendrite growth. In contrast, the SEI layer formed by LiTFSI-IL-P(VDF-HFP) gel electrolyte has a smooth and uniform surface without any dendrites or cracks (Fig. 3**e** and S12b), indicating the high performance for suppressing dendrite growth during Li^+ plating/stripping processes. The X-ray photoelectron spectroscopy (XPS) results of the SEI layers are

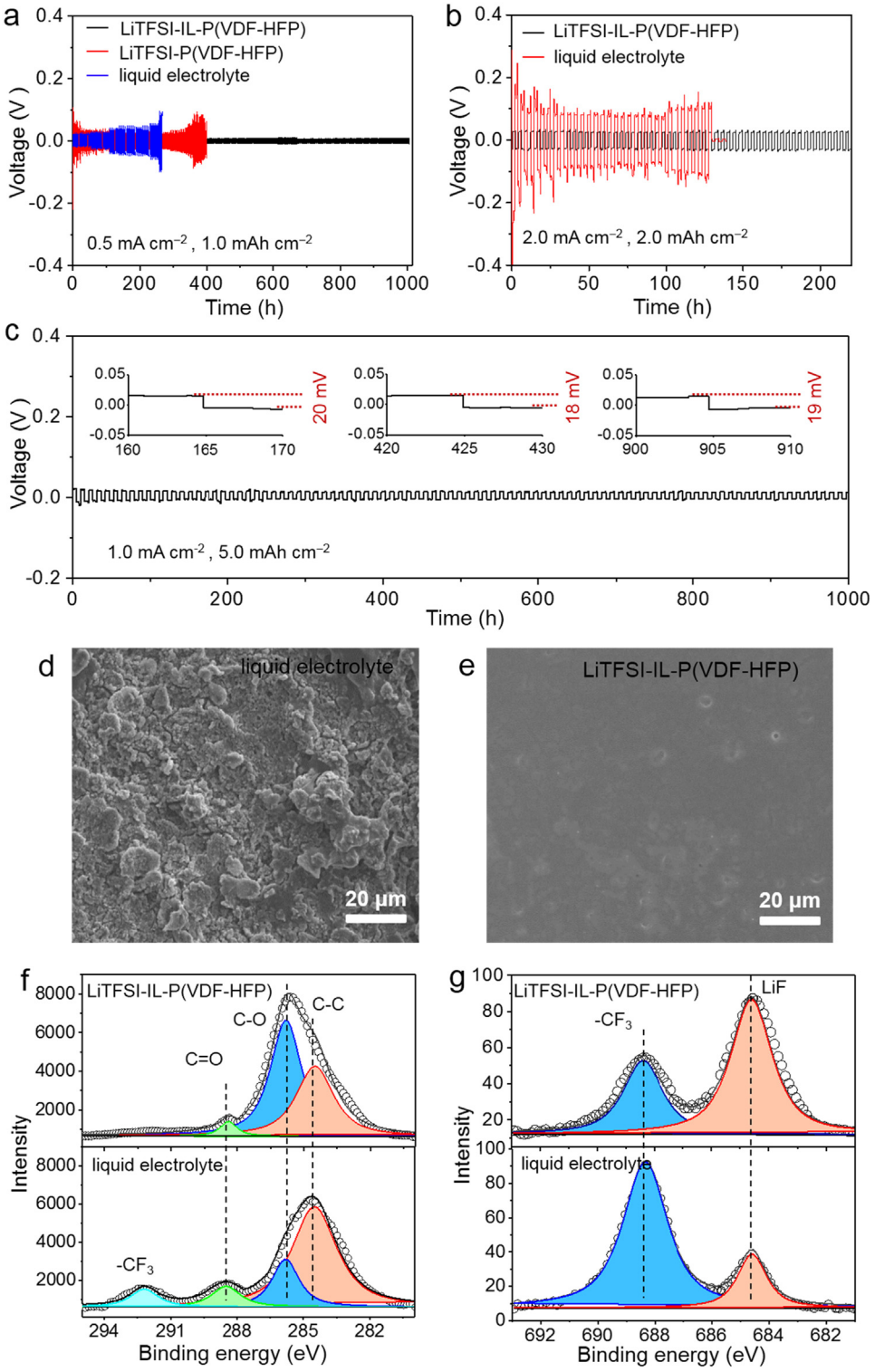

Fig. 3. (a) Li plating/stripping voltage profiles of Li/Li symmetric cells with LiTFSI-IL-P(VDF-HFP) gel, LiTFSI-P(VDF-HFP) gel, and DME/DOL-based liquid electrolytes at a current density of 0.5 mA cm^{-2} for an areal capacity of 1.0 mAh cm^{-2} per each cycle, respectively. (b) Li plating/stripping cycling stability of LiTFSI-IL-P(VDF-HFP) gel and DME/DOL-based liquid electrolytes at 2.0 mA cm^{-2} for 2.0 mAh cm^{-2} per cycle. (c) Cycling stability of LiTFSI-IL-P(VDF-HFP) gel electrolyte at 1.0 mA cm^{-2} for 5.0 mAh cm^{-2} per plating/stripping. The insets show magnified voltage profiles between the time intervals of 160–170, 420–430, and 900–910 h, respectively. SEM images of SEI layers in Li/Li symmetric cells with (d) DME/DOL-based liquid electrolyte and (e) LiTFSI-IL-P(VDF-HFP) gel electrolyte after Li plating. High-resolution XPS spectra at (f) C 1s and (g) F 1s regions of SEI layers formed by DME/DOL-based liquid electrolyte and LiTFSI-IL-P(VDF-HFP) gel electrolyte, respectively.

compared in Fig. 3**f,g**. In the C 1s XPS spectra, the peak at 292.1 and 288.5 eV was assigned to the $–CF_3$ and C=O groups, respectively, which mainly originated from the decomposition of TFSI anions and organic solvents. In the F 1s XPS spectra, the two peaks around 688.4 and 684.6 eV correspond to the formation of $–CF_3$ and LiF, respectively. For the IL-P(VDF-HFP) gel electrolyte, the peak intensity of $–CF_3$ is much lower than that of LiF. The SEI layer mainly consisted of LiF can efficiently suppress the growth of Li dendrite, as indicated by recent researches that LiF buffer layer can minimize the decomposition of organic electrolytes and restrain dendrite formation [46,47]. On the contrary, in the SEI layer of liquid electrolyte, the relative content of $–CF_3$ is higher than that of LiF, and the presence of C=O suggests the formation of Li_2CO_3, indicating the more serious electrolyte decomposition and the looser structure of SEI layer.

For applying LiTFSI-IL-P(VDF-HFP) gel electrolyte in lithium metal batteries, full cells with lithium metal anode, $LiFePO_4$ cathode and LiTFSI-IL-P(VDF-HFP) electrolyte were assembled and measured (Fig. 4**a**). Compared to the $LiFePO_4$/Li cell with conventional DME/DOL-based liquid electrolyte, the $LiFePO_4$/LiTFSI-IL-P(VDF-HFP)/Li cell showed superior rate capability (Fig. 4**b**), exhibiting high discharge

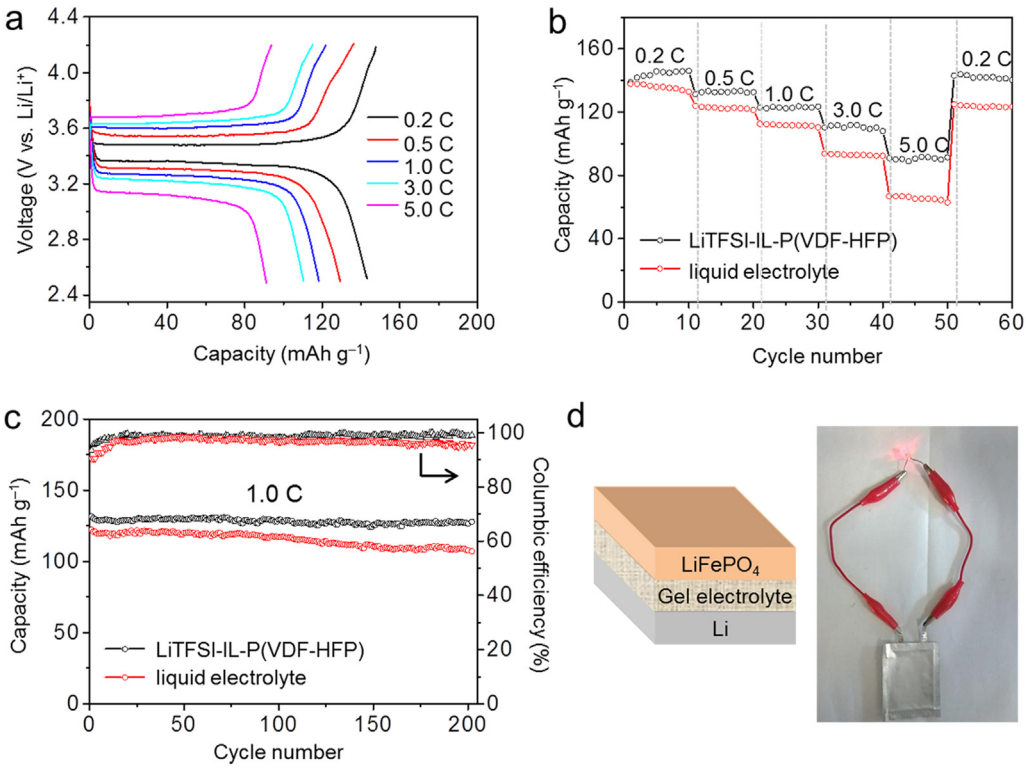

Fig. 4. (a) Voltage-capacity curves of $LiFePO_4$/LiTFSI-IL-P(VDF-HFP)/Li cell. (b) Rate capabilities and (c) long-term cycling performances of $LiFePO_4$/Li cells with LiTFSI-IL-P(VDF-HFP) gel and DME/DOL-based liquid electrolytes, respectively. (d) Structural configuration and digital photograph of $LiFePO_4$/LiTFSI-IL-P(VDF-HFP)/Li pouch cell lighting up a red LED.

capacities of 145, 133, 123, and 110 mAh g^{-1} at the current densities of 0.2, 0.5, 1.0, and 3.0 C, respectively. Notably, benefited from the high ionic conductivity and low interfacial resistance, the $LiFePO_4$/LiTFSI-IL-P(VDF-HFP)/Li cell delivered a high reversible capacity of 91 mAh g^{-1} at the high rate of 5.0 C, much higher than that of $LiFePO_4$/Li cell with liquid electrolyte (65 mAh g^{-1}) at the same rate. The $LiFePO_4$/LiTFSI-IL-P(VDF-HFP)/Li cell also showed better capacity retention than the $LiFePO_4$/Li cell with liquid electrolyte (Fig. 4**c**). The $LiFePO_4$/LiTFSI-IL-P(VDF-HFP)/Li cell delivered an initial discharge capacity of 132 mAh g^{-1} at 1.0 C, and a capacity retention of 96.5% after 200 cycles with a Coulombic efficiency of 99.8%, attributed to the good interfacial contact and dendrite-suppressed Li deposition. In comparison, the $LiFePO_4$/Li cell with liquid electrolyte delivered an initial capacity of 128.5 mAh g^{-1}, but the capacity retention and Coulombic efficiency after 200 cycles were 90.4% and 95.5%, respectively, owing to the inhomogeneous Li deposition and electrolyte decomposition near Li metal anode. Moreover, pouch cell with LiTFSI-IL-P(VDF-HFP) gel electrolyte was also assembled and tested, exhibiting its good functionality and practicability (Fig. 4**d**).

Furthermore, LiTFSI-IL-P(VDF-HFP) gel electrolyte (without $LiNO_3$ additive) was introduced into Li-S batteries to investigate its properties for preventing intermediate polysulfide shuttling effect that could cause rapid capacity decay and serious self-discharge. Commercial activated carbon (AC) with specific surface area of 2036 m^2 g^{-1} and pore volume of 0.82 cm^3 g^{-1} was used as the sulfur host (Fig. S13). The sulfur-filled AC (AC/S) composite with a sulfur content of 67 wt% (Fig. S14) was prepared by a melt-diffusion method and adopted as the cathode material. The total resistance of Li-S cell assembled with LiTFSI-IL-P(VDF-HFP) gel electrolyte is smaller than that of Li-S cell with liquid electrolyte (Fig. 5**a**). The voltage plateau differences and potential hysteresis between the discharge-charge profiles of corresponding Li-S cells at various current densities are shown in Fig. S15. The Li-S cell with LiTFSI-IL-P(VDF-HFP) gel electrolyte shows much less polarization and better reaction kinetics than that with liquid electrolyte, which is consistent with the CVs results (Fig. S16). The Li-S cell with liquid electrolyte suffers from rapid capacity decay and retains a capacity of only 490 mAh g^{-1} after 100 cycles at 0.2 C (Fig. 5**b**); while the Li-S cell with LiTFSI-IL-P(VDF-HFP) gel electrolyte delivered a stable capacity of 867 mAh g^{-1} after 200 cycles with an average Coulombic efficiency close to 100%, indicating the highly-improved capacity retention enabled by effective suppression of polysulfide shuttling. Moreover, the Li-S cell with LiTFSI-IL-P(VDF-HFP) gel electrolyte exhibits impressive improvement on rate capability (Fig. 5**c,d**), delivering high discharge capacities of 1157, 994, 859, 778, and 687 mAh g^{-1} when cycled at 0.1, 0.2, 0.5, 1.0, and 2.0 C, respectively, owing to the high ionic conductivity and low interfacial resistances.

The superiority of LiTFSI-IL-P(VDF-HFP) gel electrolyte for preventing self-discharge of Li-S batteries was investigated by two different modes (Fig. 5**e-h**) [48,49]. In the first testing mode, the Li-S cells were discharged-charged for 10 cycles, fully charged to 2.6 V and then rested for 72 h, and followed by additional 40 cycles (Fig. S17). After resting for 72 h, the Li-S cell with IL-P(VDF-HFP) gel electrolyte exhibited a low self-discharge ratio of 9.3% (Fig. 5**e**); In contrast, the Li-S cell with DME/DOL-based liquid electrolyte-soaked Celgard separator suffered from severe self-discharge with a capacity loss ratio of 21.3% (Fig. 5**f**). To further verify the effective suppression of polysulfide shuttling and the low self-discharge resulted from gel electrolyte, the Li-S cells were investigated by another testing mode (Fig. 5**g,h**). Briefly, the cells were partially charged to 2.3 V at the 5th charging step and then rested for 24 h, and followed by full discharge-charge cycles. When partially charged to 2.3 V, the sulfur species were mainly in the form of intermediate polysulfides (Li_2S_x, $4 \le x \le 8$), therefore the shuttle effect would be more obvious and severe than the fully-charged state. Remarkably, in this testing mode, a self-discharge ratio of only 7.3% was observed for the Li-S cell with IL-P(VDF-HFP) gel electrolyte, which is much lower than that with liquid electrolyte (14.5%). These results confirm that the LiTFSI-IL-P(VDF-HFP) gel electrolyte can effectively block the shuttling of polysulfide species and greatly mitigate the self-discharge phenomenon.

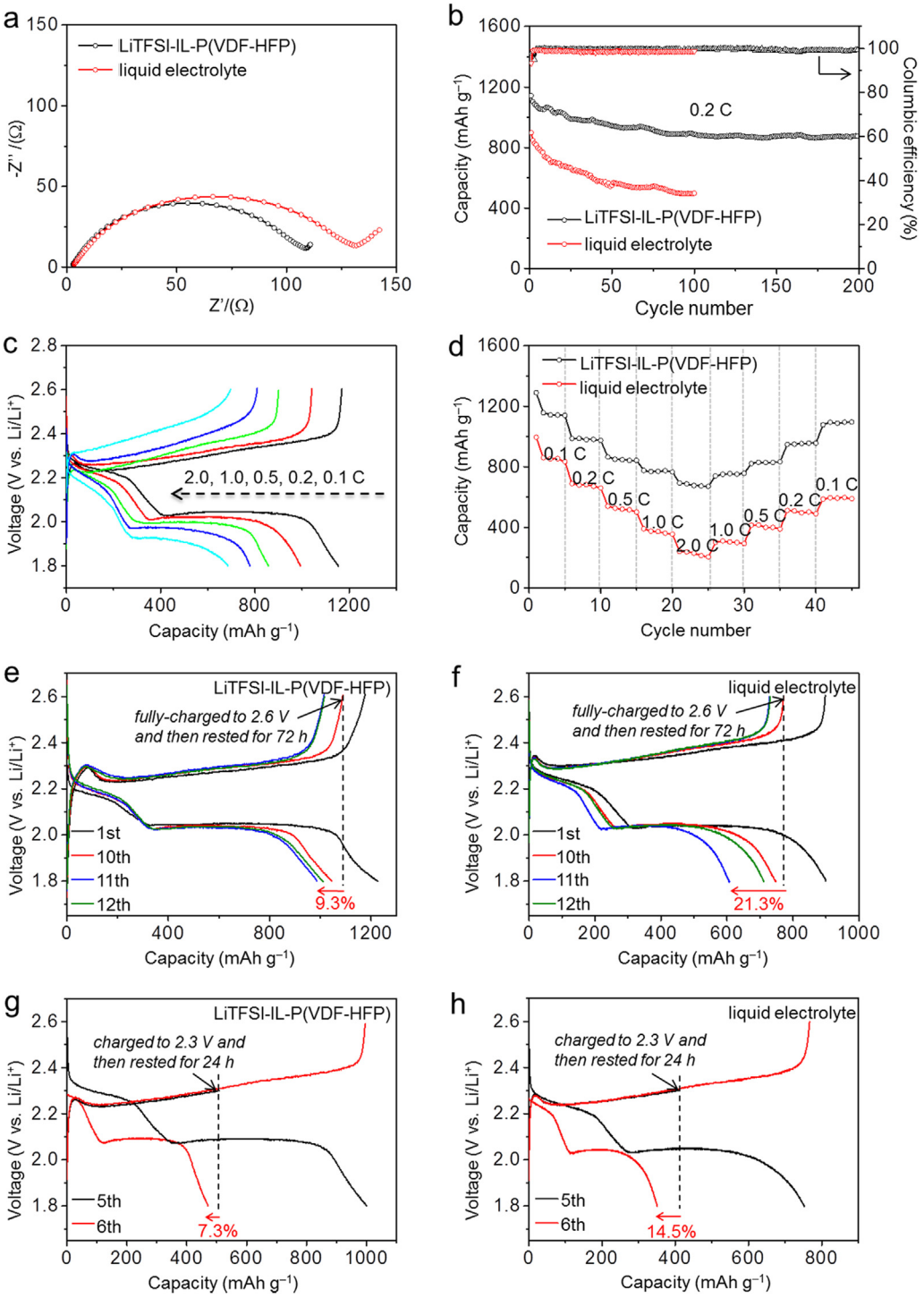

Fig. 5. (a) EIS plots and (b) cycling stability of Li-S cells with LiTFSI-IL-P (VDF-HFP) gel and DME/DOL-based liquid electrolytes. (c) Discharge-charge profiles of a Li-S cell with LiTFSI-IL-P(VDF-HFP) gel electrolyte at different current densities. (d) Rate performances of Li-S cells with LiTFSI-IL-P(VDF-HFP) gel and DME/DOL-based liquid electrolytes. (e-h) Self-discharge evaluation of Li-S batteries with (e, g) LiTFSI-IL-P(VDF-HFP) gel electrolyte and (f, h) DME/DOL-based liquid electrolyte at 0.2 C. (e, f) The Li-S cells were fully-charged to 2.6 V at the 10th cycle and then rested for 72 h. (g, h) The Li-S cells were charged to 2.3 V at the 5th cycle and then rested for 24 h.

3. Conclusion

In summary, a novel ionic liquid-immobilized polymer electrolyte has been proposed and prepared for dendrite-free Li metal batteries. The strong ion-dipole interaction of IL and copolymer matrix endows the gel electrolyte membrane with highly-improved mechanical strength, thermal stability, ionic conductivity and operation voltage window. This gel electrolyte with conducive self-healing capability can serve as a physical blocking layer to suppress the lithium dendrite growth, and also can stabilize the Li deposition by uniformizing the Li^+ distribution. The LiTFSI-IL-P(VDF-HFP) gel electrolyte enables the formation of a smooth and uniform SEI layer on lithium metal electrode, which can effectively minimize the electrolyte decomposition and restrain the dendrite growth. Consequently, the gel electrolyte can greatly enhance the cycling stability and rate performance of both $LiFePO_4$/Li and Li-S batteries. Especially, the polysulfide shuttling and self-discharge of Li-S batteries can be markedly mitigated by adopting LiTFSI-IL-P(VDF-HFP) gel electrolyte. We hope this design strategy of IL-immobilized polymer gel electrolyte can provide new insights for the construction of high-energy-density and safe lithium metal batteries.

Acknowledgements

This work was supported by National Key R&D Program of China

(2017YFA0208200, 2016YFB0700600, 2015CB659300), Projects of NSFC (21872069, 51761135104, 21573108), Natural Science Foundation of Jiangsu Province (BK20180008, BK20170644), High-Level Entrepreneurial and Innovative Talents Program of Jiangsu Province, and the Fundamental Research Funds for the Central Universities of China (020514380146).

Appendix A. Supplementary material

Supplementary data associated with this article can be found in the online version at doi:10.1016/j.nanoen.2018.09.059.

References

[1] D.C. Lin, Y.Y. Liu, Y. Cui, Nat. Nanotechnol. 12 (2017) 194–206.
[2] J.-M. Tarascon, M. Armand, Nature 414 (2001) 359–367.
[3] W. Xu, J.L. Wang, F. Ding, X.L. Chen, E. Nasybulin, Y.H. Zhang, J.G. Zhang, Energy Environ. Sci. 7 (2014) 513–537.
[4] Y. Lu, Z. Tu, L.A. Archer, Nat. Mater. 13 (2014) 961–969.
[5] K.J. Harry, D.T. Hallinan, D.Y. Parkinson, A.A. Macdowell, N.P. Balsara, Nat. Mater. 13 (2014) 69–73.
[6] X.B. Cheng, R. Zhang, C.Z. Zhao, F. Wei, J.G. Zhang, Q. Zhang, Adv. Sci. 3 (2015) 1500213.
[7] G.Y. Zheng, S.W. Lee, Z. Liang, H.-W. Lee, K. Yan, H. Yao, H.T. Wang, W.Y. Li, S. Chu, Y. Cui, Nat. Nanotechnol. 9 (2014) 618–623.
[8] D.C. Lin, J. Zhao, J. Sun, H.B. Yao, Y.Y. Liu, K. Yan, Y. Cui, Proc. Natl. Acad. Sci. USA 114 (2017) 4613–4618.
[9] J.M. Zheng, M.H. Engelhard, D.H. Mei, S.H. Jiao, B.J. Pozin, J.G. Zhang, W. Xu, Nat. Energy 2 (2017) 17012.
[10] N.W. Li, Y.X. Yin, C.P. Yang, Y.G. Guo, Adv. Mater. 28 (2016) 1853–1858.
[11] R. Bouchet, S. Maria, R. Meziane, A. Aboulaich, L. Livie, J.-P. Bonnet, T.N.T. Phan, D. Bertin, D. Gigmes, D. Devaux, R. Denoyel, M. Armand, Nat. Mater. 12 (2013) 452–457.
[12] X. Zhang, T. Liu, S.F. Zhang, X. Huang, B.Q. Xu, Y.H. Lin, B. Xu, L.L. Li, C.W. Nan, Y. Shen, J. Am. Chem. Soc. 139 (2017) 13779–13785.
[13] S. Choudhury, R. Mangal, A. Agrawal, L.A. Archer, Nat. Commun. 6 (2015) 10101.
[14] C.W. Sun, J. Liu, Y.D. Gong, D.P. Wilkinson, J.J. Zhang, Nano Energy 33 (2017) 363–386.
[15] S.Q. Li, D. Zhang, X.Y. Meng, Q.A. Huang, C.W. Sun, Z.L. Wang, Energy Storage Mater. 12 (2018) 17–22.
[16] W.Q. Zhang, J.H. Nie, F. Li, Z.L. Wang, C.W. Sun, Nano Energy 45 (2018) 413–419.
[17] H.D. Hou, Q.K. Xu, Y.K. Pang, L. Li, J.L. Wang, C. Zhang, C.W. Sun, Adv. Sci. 4 (2017) 1700072.
[18] W. Luo, L.H. Zhou, K. Fu, Z. Yang, J.Y. Wan, M. Manno, Y.G. Yao, H.L. Zhu, B. Yang, L.B. Hu, Nano Lett. 15 (2015) 6149–6154.
[19] D. Lin, D. Zhuo, Y.Y. Liu, Y. Cui, J. Am. Chem. Soc. 138 (2016) 11044–11050.
[20] D. Lin, Y.Y. Liu, Y. Cui, Nat. Nanotechnol. 11 (2016) 626–632.
[21] K. Yan, Z.D. Lu, H.-W. Lee, F. Xiong, P.-C. Hsu, Y.Z. Li, J. Zhao, S. Chu, Y. Cui, Nat. Energy 1 (2016) 16010.
[22] C.P. Yang, Y.X. Yin, S.F. Zhang, N.W. Li, Y.G. Guo, Nat. Commun. 6 (2015) 8058.
[23] Z.Q. Zhu, M.L. Hong, D.S. Guo, J.F. Shi, Z.L. Tao, J. Chen, J. Am. Chem. Soc. 136 (2014) 16461–16464.
[24] W.D. Zhou, S.F. Wang, Y.T. Li, S. Xin, A. Manthiram, J.B. Goodenough, J. Am. Chem. Soc. 138 (2016) 9385–9388.
[25] Q.W. Lu, Y.B. He, Q.P. Yu, B.H. Li, Y.V. Kaneti, Y.W. Yao, F.Y. Kang, Q.H. Yang, Adv. Mater. 29 (2017) 1604460.
[26] S. Shim, H.J. Kim, B.G. Kim, Y.S. Kim, D.-G. Kim, J.-C. Lee, Energy Environ. Sci. 10 (2017) 1911–1916.
[27] M. Liu, D. Zhou, Y.B. He, Y.Z. Fu, X.Y. Qin, C. Miao, H.D. Du, B.H. Li, Q.H. Yang, Z.Q. Lin, T.S. Zhao, F.Y. Kang, Nano Energy 22 (2016) 278–289.
[28] S. Ferraria, E. Quartaronea, P. Mustarellia, A. Magistrisa, M. Fagnonib, S. Prottib, C. Gerbaldic, A. Spinella, J. Power Sources 195 (2010) 559–566.
[29] H. Ye, J. Huang, J.J. Xu, A. Khalfan, S.G. Greenbaum, J. Electrochem. Soc. 154 (2007) A1048–A1057.
[30] J. Fuller, A.C. Breda, R.T. Carlin, J. Electrochem. Soc. 144 (1997) L67–L70.
[31] D.C. Lin, W. Liu, Y.Y. Liu, H.R. Lee, P.-C. Hsu, K. Liu, Y. Cui, Nano Lett. 16 (2016) 459–465.
[32] G.Q. Tan, F. Wu, C. Zhan, J. Wang, D.B. Mu, J. Lu, K. Amine, Nano Lett. 16 (2016) 1960–1968.
[33] A. Guyomard-Lack, J. Abusleme, P. Soudan, B. Lestriez, D. Guyomard, J.L. Bideau, Adv. Energy Mater. 4 (2014) 1301570.
[34] F. Croce, G.B. Appetecchi, L. Persi, B. Scrosati, Nature 394 (1998) 456–458.
[35] I. Gurevitch, R. Buonsanti, A.A. Teran, B. Buonsanti, R.O. Ritchie, J. Buonsanti, N.P. Balsara, J. Electrochem. Soc. 160 (2013) A1611–A1617.
[36] Y. Lu, K. Korf, Y. Kambe, Z. Tu, L.A. Archer, Angew. Chem. Int. Ed. 53 (2014) 488–492.
[37] Y. Lu, S.K. Das, S.S. Moganty, L.A. Archer, Adv. Mater. 24 (2012) 4430–4435.
[38] M.D. Tikekar, L.A. Archer, D.L. Koch, Sci. Adv. 2 (2016) e1600320.
[39] Z. Tu, P. Nath, Y. Lu, M.D. Tikekar, L.A. Archer, Acc. Chem. Res. 48 (2015) 2947–2956.
[40] W.Y. Li, H.B. Yao, K. Yan, G.Y. Zheng, Z. Liang, Y.-M. Chiang, Y. Cui, Nat. Commun. 3 (2015) 7436.
[41] J. Dupont, R.F. de Souza, P.A.Z. Suarez, Chem. Rev. 102 (2002) 3667–3692.
[42] R. Rohan, K. Pareek, Z.X. Chen, W.W. Cai, Y.F. Zhang, G.D. Xu, Z.Q. Gao, H.S. Cheng, J. Mater. Chem. A 3 (2015) 20267–20276.
[43] Y. Cao, T. Morrissey, E. Acome, S.I. Allec, B.M. Wong, C. Keplinger, C. Wang, Adv. Mater. 29 (2016) 1605099.
[44] Z. Li, G. Su, D. Gao, X. Wang, X. Li, Electrochim. Acta 49 (2004) 4633–4639.
[45] G.M. Stone, S.A. Mullin, A.A. Teran, D.T. Hallinan, A.M. Minor, A. Hexemer, N.P. Balsara, J. Electrochem. Soc. 159 (2012) A222–A227.
[46] M.D. Tikekar, S. Choudhury, Z.Y. Tu, L.A. Archer, Nat. Energy 1 (2016) 1–7.
[47] J. Zhao, L. Liao, F.F. Shi, T. Lei, G.X. Chen, A. Pei, J. Sun, K. Yan, G.M. Zhou, J. Xie, C. Liu, Y.Z. Li, Z. Liang, Z.N. Bao, Y. Cui, J. Am. Chem. Soc. 139 (2017) 11550–11558.
[48] L.N. Wang, J.Y. Liu, S.Y. Yuan, Y.G. Wang, Y.Y. Xia, Energy Environ. Sci. 9 (2016) 224–231.
[49] Y. Pang, J.S. Wei, Y.G. Wang, Y.Y. Xia, Adv. Energy Mater. (2018) 1702288.

Tao Chen received his Ph.D. degree in Chemical Engineering and Technology under supervision of Prof. Jiajun Fu from Nanjing University of Science and Technology in June 2015. He is currently a postdoctoral researcher in the group of Prof. Zhong Jin and Prof. Jie Liu at Nanjing University. His current research focuses on the design and synthesis of nanostructured electrode materials for rechargeable batteries.

Weihua Kong received his B.S. degree in Chemistry from Hunan University in 2017. He is now pursuing his M.S degree under the supervision of Prof. Zhong Jin in College of Chemistry and Chemical Engineering at Nanjing University. His research interest is mainly concentrated on the nanomaterials for metal-sulfur batteries.

Zewen Zhang received his Bachelor's degree from School of Chemistry and Chemical Engineering, Nanjing University in 2018. He is currently pursuing his master degree under the supervision of Prof. Zhong Jin and Prof. Jie Liu at the same school. His research interests focus on improving properties of lithium metal batteries and hydrogen storage materials.

Lei Wang obtained his B.S. degree in chemistry from Jiangsu University in 2016. He is now pursuing his M.S. degree under the supervision of Professor Zhong Jin in School of Chemistry and Chemical Engineering at Nanjing University. His research interest is focused on rechargeable aluminum-ion battery.

Yi Hu received his B.S. degree in Chemistry from Sichuan University in 2014. He is now pursuing his Ph.D. degree under the supervision of Prof. Zhong Jin in School of Chemistry and Chemical Engineering at Nanjing University. His research interests reside in two-dimensional nanomaterials for electrochemical energy storage and photoelectric conversion.

Guoyin Zhu obtained his M.S. degree from Nanjing University of Posts & Telecommunications in 2014. Currently, he is pursuing his Ph.D. degree under the supervision of Prof. Zhong Jin and Jie Liu at Nanjing University. His research is mainly focused on the synthesis of carbonaceous nanomaterials, and their application for energy conversion and storage devices.

Renpeng Chen has graduated from the Northeastern University (China) since 2014. Now, he is pursuing his M.S. degree under the guidance of Prof. Zhong Jin in School of Chemistry and Chemical Engineering at Nanjing University. His research interest is focused on the synthesis of alloy materials for lithium-ion batteries.

Lianbo Ma received his M.S. degree in Applied Chemistry from Jiangsu University, PR China (2015). He is now pursing his Ph.D. degree under the supervision of Prof. Zhong Jin and Jie Liu in School of Chemistry and Chemical Engineering, Nanjing University, P.R. China. His main interest is the design and fabrication nanomaterials for photoelectric conversion.

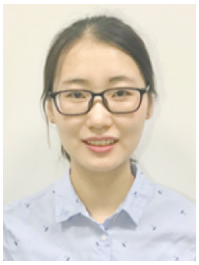

Wen Yan received her B.S. degree from Nanjing University in 2016. She is now pursuing her Ph.D. degree under the supervision of Prof. Zhong Jin and Prof. Jie Liu at Nanjing University. Her research interest focuses on the application of polymers and organic framework materials for energy conversion and storage devices.

Yanrong Wang received her master degree in physical chemistry under the supervision of Professor Yong Hu in College of Chemistry and life sciences at Zhejiang Normal University in 2015. She is now pursuing her Ph.D. degree under the supervision of Prof. Zhong Jin and Jie Liu in School of Chemistry and Chemical Engineering at Nanjing University. Her current research interest is the design of new type of battery.

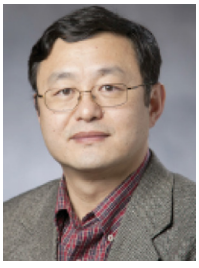

Jie Liu is currently the George B. Geller Professor of Chemistry at Duke University and an adjunct professor of "Thousands Talents" Program at Nanjing University. He earned a B.S. from Shandong University in 1987 and a Ph.D. from Harvard University in 1996. His research interests include the synthesis and chemical functionalization of nanomaterials, nanoelectronic devices, scanning probe microscopy, and carbon nanomaterials. Prof. Liu is a Fellow of the AAAS, APS and RSC.

Zhong Jin received his B.S. (2003) and Ph.D. (2008) in chemistry from Peking University. He worked as a postdoctoral scholar at Rice University and Massachusetts Institute of Technology. Now he is a professor in School of Chemistry and Chemical Engineering at Nanjing University. He leads a research group working on advanced materials and devices for energy conversion and storage.